Supporting Information

Asymmetric Glycolated Substitution for Enhanced Permittivity and Ecocompatibility of High-Performance Photovoltaic Electron Acceptor

Tengfei Li,[a] Kang Wang,[b] Guilong Cai,[c] Yawen Li,[a] Heng Liu,[c] Yixiao Jia,[a] Zhenzhen Zhang,[a d] Xinhui Lu,[c] Ye Yang,[* b] and Yuze Lin[* a d]

[a] Beijing National Laboratory for Molecular Sciences, CAS Key Laboratory of Organic Solids, Institute of Chemistry, Chinese Academy of Sciences, Beijing 100190, China

[b] State Key Laboratory of Physical Chemistry of Solid Surfaces, College of Chemistry and Chemical Engineering, Xiamen University, Xiamen 361005, China

[c] Department of Physics, The Chinese University of Hong Kong, New Territories 999077, Hong Kong, China

[d] University of Chinese Academy of Sciences, Beijing 100049, China

* Corresponding Authors: linyz@iccas.ac.cn (Y.L.), ye.yang@xmu.edu.cn (Y.Y.)

Materials

Unless stated otherwise, all the solvents and chemical reagents used were obtained commercially and used without further purification. Compound 1 and compound 5 were purchased from Innochem Co., Ltd.; compound 3 and 2-(5, 6-difluoro-3-oxo-2,3-dihydro-1H-inden-1-ylidene) malononitrile (2FIC) were purchased from Hyper Inc. PM6 was purchased from Solarmer Materials Inc.; Y6 was purchased from eFlexPV Ltd.; PDINN was synthesized according to the literature procedure.[1]

Synthesis

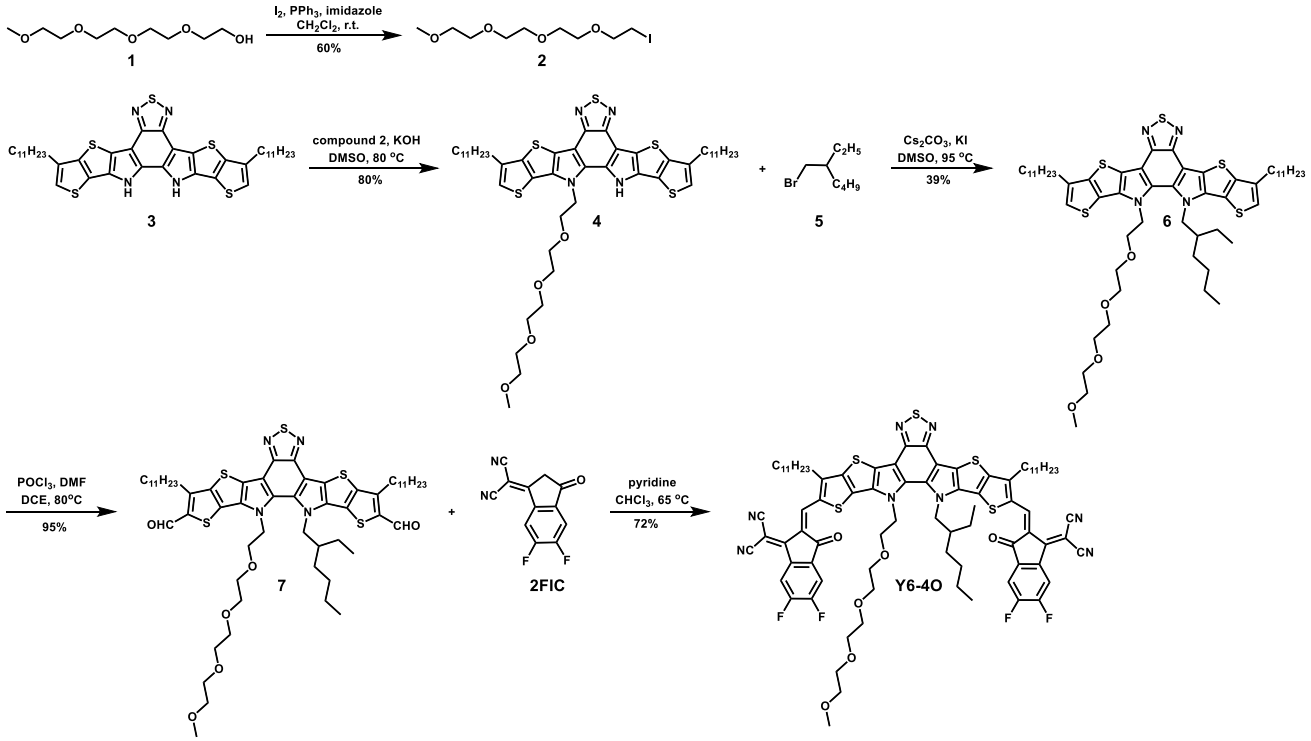

Scheme S1. Synthetic route for Y6-4O.

Compound 2. To a three-necked round bottom flask, PPh_3 (3.9 g, 15 mmol), I_2 (3.8 g, 15 mmol), imidazole (1.8 g, 26 mmol) and dichloromethane (CH_2Cl_2) (30 mL) were added. The mixture was stirred at room temperature for 10 min, and then compound 1 (2.1 g, 10 mmol) was added. The mixture was stirred overnight at room temperature. Brine (30 mL) was added and the mixture was extracted with dichloromethane (2 × 30 mL). The organic phase was dried over anhydrous Na_2SO_4 and filtered. After removing the solvent from the filtrate, the residue was redissolved in petroleum

ether and filtered. The product was obtained after removing the solvent from the filtrate as a yellowish oil (1.9 g, 60%). ^{1}H NMR (300 MHz, CD_2Cl_2): δ 3.70 (t, J = 7.5 Hz, 3H), 3.60 (m, 10H), 3.49 (m, 2H), 3.32 (s, 3H), 3.20 (t, J = 7.5 Hz, 3H). ^{13}C NMR (75 MHz, $CDCl_3$): δ 71.80, 71.79, 70.50, 70.47, 70.45, 70.38, 70.20, 70.06, 58.91, 58.88. MS (MALDI-TOF): *m/z* 318.0 (M^+).

Compound 4. To a three-necked round bottom flask, compound 3 (224 mg, 0.3 mmol), compound 2 (286 mg, 0.9 mmol), KOH (168 mg, 3 mmol) and DMSO (8 mL) were added. After deoxygenated with nitrogen for 15 min, the mixture was stirred at 80 °C for 20 h and then cooled down to room temperature. Brine (30 mL) was added and the mixture was extracted with dichloromethane (2 × 30 mL). The organic phase was dried over anhydrous Na_2SO_4 and filtered. After removing the solvent from the filtrate, the residue was purified by column chromatography on silica gel using CH_2Cl_2/ethyl acetate (100:1) as the eluent yielding a red solid (crude yield: 224 mg, 80%). MS (MALDI-TOF): *m/z* 936.6 (M^+).

Compound 6. To a three-necked round bottom flask, compound 4 (187 mg, 0.2 mmol), compound 5 (193 mg, 1 mmol), KI (33 mg, 0.2 mmol), Cs_2CO_3 (651 mg, 2 mmol), and DMSO (10 mL) were added. After deoxygenated with nitrogen for 15 min, the mixture was stirred at 95 °C for 36 h and then cooled down to room temperature. Brine (30 mL) was added and the mixture was extracted with dichloromethane (2 × 30 mL). The organic phase was dried over anhydrous Na_2SO_4 and filtered. After removing the solvent from the filtrate, the residue was purified by column chromatography on silica gel using CH_2Cl_2/ethyl acetate (100:1) as the eluent yielding a red solid (82 mg, 39%). ^{1}H NMR (400 MHz, $CDCl_3$): δ 7.05 (s, 2H), 4.85 (t, J = 4.8 Hz, 2H), 4.64 (m, 2H), 3.70 (t, J = 4.8 Hz, 2H), 3.45 (m, 4H), 3.31 (m, 4H), 3.25 (m, 4H), 3.18 (m, 2H), 2.81 (t, J = 5.7 Hz, 3H), 2.05 (m, 1H), 1.85 (m, 4H), 1.27 (m, 36 H), 0.88 (m, 12 H), 0.61 (m, 6H). MS (MALDI-TOF): *m/z*

1048.8 (M^+).

Compound 7. To a three-necked round bottom flask were added $POCl_3$ (0.5 mL) and DMF (2.5 mL) under the protection of nitrogen and the solution was stirred at 0 °C for 2 h. Then, compound 6 (105 mg, 0.1 mmol) in 1,2-dichloroethane solution (15 mL) was added. After stirred at 80 °C for 12 h, the mixture was quenched with saturated CH_3COONa (aq) and extracted with dichloromethane (2 × 30 mL). The organic phase was dried over anhydrous $MgSO_4$ and filtered. After removing the solvent from the filtrate, the residue was purified by column chromatography on silica gel using CH_2Cl_2/ethyl acetate (50:1) as the eluent yielding an orange solid (105 mg, 95%). ^{1}H NMR (500 MHz, $CDCl_3$): δ 10.1 (s, 2H), 4.89 (t, J = 5.5 Hz, 2H), 4.68 (m, 2H), 3.74 (t, J = 5.5 Hz, 2H), 3.45 (m, 4H), 3.31 (m, 4H), 3.26 (m, 2H), 3.19 (m, 4H), 3.16 (m, 3H), 2.03 (m, 1H), 1.92 (m, 4H), 1.71 (m, 2H), 1.45 (m, 4H), 1.37 (m, 4 H), 1.26 (m, 24H), 0.96 (m, 6H), 0.87 (m, 8H), 0.68 (m, 3H), 0.60 (m, 3H). ^{13}C NMR (125 MHz, $CDCl_3$): δ 181.83, 181.78, 147.59, 147.42, 146.86, 143.15, 137.07, 137.02, 136.84, 136.71, 133.48, 132.78, 132.36, 130.96, 129.74, 129.41, 128.89, 129.09, 127.10, 112.93, 112.30, 71.85, 70.83, 70.43, 70.35, 69.61, 65.61, 59.02, 55.20, 50.90, 40.27, 31.95, 30.62, 30.40, 30.38, 29.75, 29.71, 29.68, 29.65, 29.62, 29.57, 29.42, 29.37, 28.22, 28.19, 27.62, 23.16, 22.73, 19.24, 14.17, 13.78, 13.71, 10.18. MS (MALDI-TOF): *m/z* 1104.7 (M^+).

Y6-4O. To a three-necked round bottom flask were added compound 7 (110 mg, 0.1 mmol), 2FIC (97 mg, 0.4 mmol), pyridine (0.3 mL) and chloroform ($CHCl_3$) (20 mL). The mixture was deoxygenated with nitrogen for 15 min and then stirred at reflux for 12 h. After cooling down to room temperature, the mixture was poured into methanol (150 mL) and filtered. The residue was purified by column chromatography on silica gel using CH_2Cl_2/ethyl acetate (50:1) as eluent yielding a purple solid (110 mg, 72%). ^{1}H NMR (400 MHz, $CDCl_3$): δ 8.98 (s, 1H), 8.93 (s, 1H), 8.50 (m,

2H), 7.66 (m, 2H), 5.03 (m, 2H), 4.78 (m, 2H), 4.04 (m, 2H), 3.48 (m, 4H), 3.44 (m, 2H), 3.37 (m, 4H), 3.29 (m, 4H), 3.11 (m, 3H), 2.03 (m, 1H), 1.82 (m, 6H), 1.71 (m, 2H), 1.49 (m, 4H), 1.26 (m, 30 H), 1.01 (m, 4H), 0.87 (m, 6H), 0.74 (t, J = 7.2 Hz, 3H), 0.65 (t, J = 7.2 Hz, 3H). ^{13}C NMR (100 MHz, $CDCl_3$): δ 186.09, 185.87, 158.30, 158.10, 155.61, 155.51, 153.83, 153.64, 153.04, 152.90, 147.30, 147.25, 145.27, 145.14, 137.50, 137.30, 136.49, 135.55, 135.23, 134.62, 134.52, 134.33, 133.67, 133.11, 132.90, 130.90, 130.44, 129.84, 119.85, 119.71, 114.88, 114.82, 114.60, 114.55, 113.65, 113.55, 112.23, 112.20, 72.01, 71.96, 71.17, 70.61, 70.57, 70.52, 70.09, 68.91, 68.86, 64.63, 62.85, 59.07, 55.67, 54.26, 51.14, 40.80, 32.02, 31.16, 31.14, 29.94, 29.89, 29.75, 29.73, 29.62, 29.59, 29.53, 29.45, 28.07, 25.48, 23.50, 22.89, 22.79, 14.21, 13.84, 13.80, 10.57, 10.48. MS (MALDI-TOF): *m/z* 1530.7 (MH^+).

Characterization

The ^{1}H and ^{13}C NMR spectra were obtained using a Bruker AVANCE 300 MHz and 400 MHz spectrometer. The MALDI-TOF mass spectrometry experiments were performed on an autoflex III instrument (Bruker Daltonics, Inc.). UV-vis absorption spectra (solution in $CHCl_3$; thin film on quartz substrate) were measured on a UH4150 Spectrophotometer. Ultraviolet photoelectron spectroscopy (UPS) spectra were obtained from AXIS ULTRA DLD (Kratos) with He I (21.22 eV) excitation lines and a sample bias of –9 V under a vacuum of 3.0×10^{-8} Torr. Low-energy inverse photoemission spectroscopy (LEIPS) measurement was performed on a customized ULVAC-PHI LEIPS instrument with Bremsstrahlung isochromatic mode. Density functional theory (DFT) analysis with the B3LYP/6-31G (d, p) basis set was performed.

The dielectric constant was determined by the parallel-plate-capacitance measurement with a device structure of ITO/PEDOT:PSS/test film/Ca/Al. A thin layer (30 nm) of

poly(3,4-ethylenedioxythiophene):poly(styrene sulfonate) (PEDOT:PSS, Baytron PVP AI 4083, Germany) was spin-coated at 4000 rpm onto the ITO glass and then baked at 150 °C for 15 min. Y6 was dissolved in $CHCl_3$ (20 mg mL^{-1}) and spin-coated at 2000 rpm to form the test film (*ca.* 120 nm). Y6-4O was dissolved in toluene (25 mg mL^{-1}) and spin-coated at 1600 rpm to form the test film (*ca.* 120 nm). PM6 was dissolved in toluene (15 mg mL^{-1}) and spin-coated at 1600 rpm to form the test film (*ca.* 120 nm). Then, the Ca layer (*ca.* 20 nm) and Al layer (*ca.* 60 nm) were subsequently evaporated onto the surface of the test film under vacuum (*ca.* 10^{-5} Pa). The measurement was performed using a Keysight E4980A LCR meter by sweeping the frequency from 0.1 to 1000 kHz.

Atomic force microscopy (AFM) images were recorded using a Digital Instruments Nano scope IIIa multimode atomic force microscope in tapping mode under ambient conditions. The grazing incidence X-ray scattering measurements (GIWAXS and GISAXS) were carried out with a Xeuss 2.0 SAXS/WAXS laboratory beamline using a Cu X-ray source (8.05 keV, 1.54 Å) and a Pilatus3R 300K detector. The incidence angle is 0.2°. Both GIWAXS and GISAXS samples are prepared on silicon substrate by spin coating. The *d*-spacing (*d*) of molecular stacking can be calculated by the equation: $d = 2\pi/q$.[2]

Electroluminescence (EL) measurements were performed by an integrated system (REPS, Enli Technology Co., Ltd.).

Fourier-transform photocurrent spectroscopy external quantum efficiency (FTPS-EQE) were obtained on an integrated system (PECT-600, Enli Technology Co., Ltd.), where the photocurrent was amplified and modulated by a lock-in instrument.

Device fabrication and characterization

The structure of OSCs was ITO/PEDOT:PSS/active layer/PDINN/Ag. Patterned ITO glass

(sheet resistance = 15 Ω) was precleaned in an ultrasonic bath with ultra-pure water, acetone and isopropanol, and treated in an ultraviolet–ozone chamber (Mondel UV-03 UVO_3 cleaner) for 20 min. PEDOT:PSS layer (*ca.* 30 nm) was spin-coated at 4000 rpm onto the ITO glass and then baked at 150 °C for 15 min. For single component devices, Y6 was dissolved in $CHCl_3$ (20 mg mL^{-1}) and spin-coated at 2000 rpm to form the active layer (*ca.* 120 nm). Y6-4O was dissolved in toluene (25 mg mL^{-1}) and spin-coated at 1600 rpm to form the active layer (*ca.* 120 nm). For binary-blend devices, PM6:Y6 or PM6:Y6-4O (1:1.2, weight ratio) were dissolved in toluene (18 mg mL^{-1} in total) and spin-coated at 2400 rpm for 40 s to form the photoactive layers (*ca.* 110 nm). PM6:Y6-4O (1:1.2, weight ratio) were dissolved in xylene (20 mg mL^{-1} in total) and spin-coated at 2000 rpm for 40 s to form the photoactive layers (*ca.* 110 nm). PM6:Y6-4O (1:1.2, weight ratio) were dissolved in THF (16 mg mL^{-1} in total) and spin-coated at 3000 rpm for 40 s to form the photoactive layers (*ca.* 110 nm). The PDINN solution (1 mg mL^{-1} in methanol) was spin-coated on the active layer at 3600 rpm for 30 s. Finally, Ag electrode (*ca*. 80 nm) was slowly evaporated onto the surface of the photoactive layer under vacuum (*ca*. 10^{-5} Pa). The active area of the device was *ca.* 4 mm^2. The devices were not masked and the active area of devices was measured by optical microscopy. The *J*–*V* curves were measured under AM 1.5G illumination at 100 mW cm^{-2} using an AAA solar simulator (XES-70S1, SAN-EI Electric Co., Ltd) calibrated with a standard photovoltaic cell equipped with a KG5 filter (certificated by the National Institute of Metrology) and a Keithley 2450 source-measure unit. The EQE spectrum was measured using Solar Cell Spectral Response Measurement System QE-R3011 (Enlitech Co., Ltd.). The light intensity at each wavelength was calibrated using a standard single crystal Si photovoltaic cell.

Femtosecond transient absorption

The femtosecond transient absorption (TA) measurement is based on the Ti Sapphire laser system (Coherent, Astrella, center wavelength ~800 nm, pulse duration ~35 fs, ~7mJ/pulse and 1kHz repetition rate). The output laser pulse trains of 800 nm were divided into two beams by a beam splitter. One was sent to a TOPAS optical parameter amplifiers (OPA) to generate the pump light and its intensity was attenuated by two neutral density filter wheels. The other beam was focused onto sapphire windows to generated the continuous visible probe light (420-780 nm) and near-IR probe light (780-1300 nm). The pump light was chopped by a frequency of 500 Hz and the probe light was delayed by mechanical stage up to ~5 ns. After that the pump and probe light were focused and overlapped on the sample in time and space. The beam size of pump and probe light at samples is 550 μm and 200 μm, respectively. The as-used power density was controlled to 13.5 mW/cm^2. All of tests were carried out in a vacuum cell (10^{-2} Pa).

Mobility measurements

Electron-only devices were fabricated using the architectures of ITO/ZnO/active layer (acceptor or PM6:acceptor)/Ca/Al. The active layer was formed through the same preparation condition as the photovoltaic devices. Then, Ca (*ca.* 20 nm) and Al (*ca.* 60 nm) were evaporated under vacuum (*ca.* 10^{-5} Pa). Hole-only devices were fabricated using the architecture of ITO/PEDOT:PSS/PM6:acceptor/Au. The PEDOT:PSS layer and active layer were formed through the same preparation condition as the photovoltaic devices. Then, Au (*ca*. 30 nm) was evaporated under vacuum (*ca*. 10^{-5} Pa) at a low speed (1 Å/5 s) to avoid the penetration of Au atoms into the active layer. The mobility was extracted by fitting the current density–voltage curves using SCLC.[3] The formula is as follows.

$$J = \frac{9}{8}\mu\varepsilon_0\varepsilon_r\frac{V^2}{d^3} \qquad \text{(S1)}$$

where J is current density, μ is hole or electron mobility, ε_r is relative dielectric constant (the average values of ε_r at the frequency of 1 kHz was used for the calculation here), ε_0 is permittivity of free space, $V = V_{appl} - V_{bi}$, where V_{appl} is the applied voltage to the device, and V_{bi} is the built-in voltage due to the difference in work function of the two electrodes (for hole-only diodes, V_{bi} is 0.2 V; for electron-only diodes, V_{bi} is 0 V). d is the thickness of organic layer. The thickness of organic layer was measured on DektakXT (Bruker).

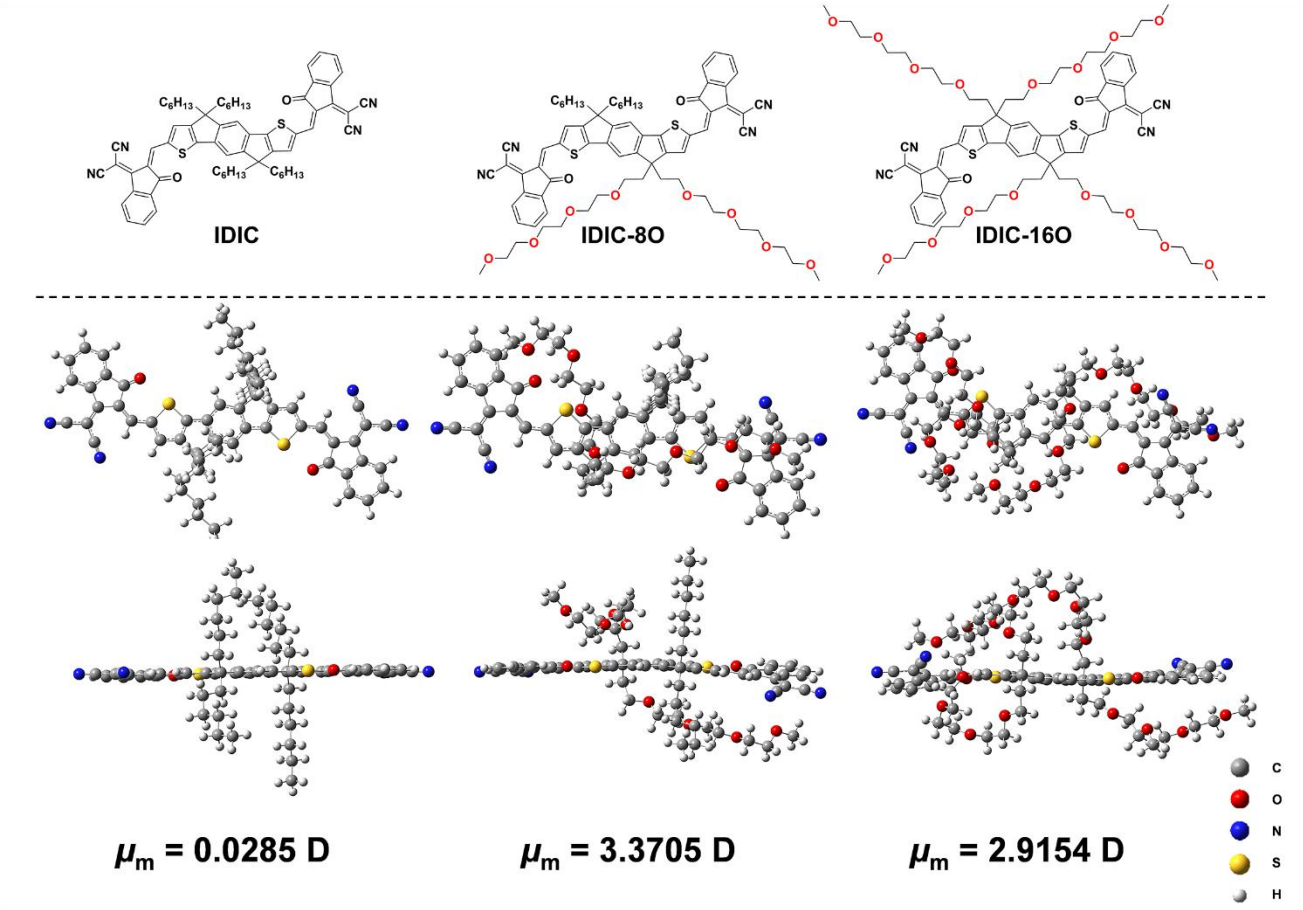

Figure S1. The optimal geometries of IDIC, IDIC-8O and IDIC-16O calculated by Gaussian 09 program at B3LYP/6-31G* level (top: top view, bottom: side view).

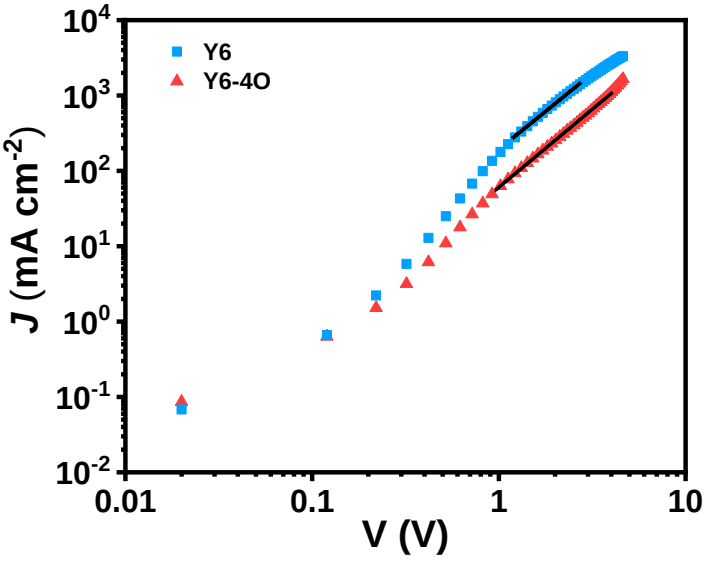

Figure S2. *J-V* characteristics in the dark for electron-only devices based on Y6 and Y6-4O.

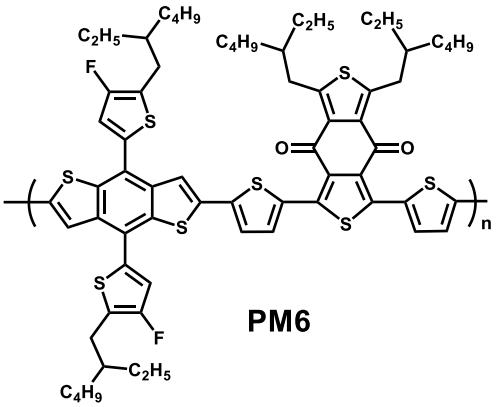

Figure S3. The chemical structure of PM6.

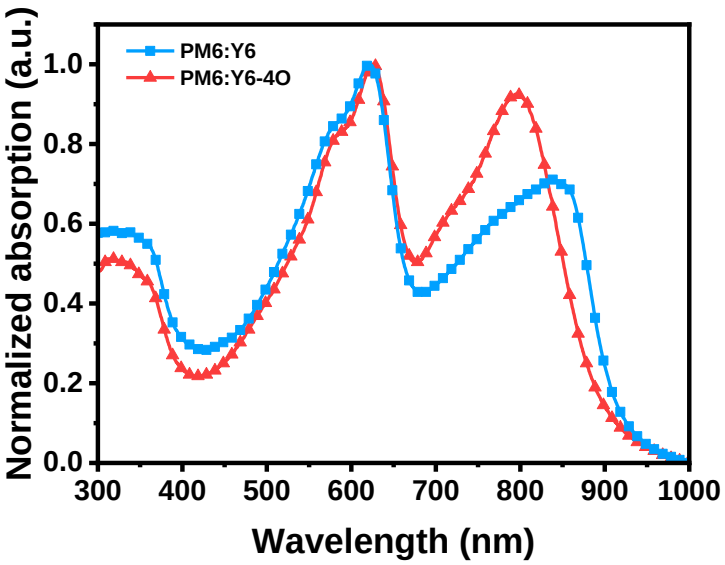

Figure S4. The absorption spectra of PM6:Y6 and PM6:Y6-4O blend films processed from toluene.

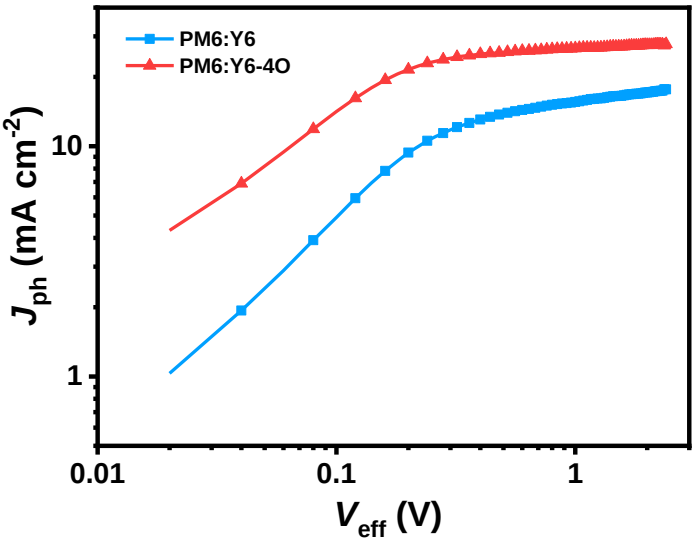

Figure S5. J_{ph} versus V_{eff} characteristics of the as-cast devices processed from toluene based on PM6:Y6 and PM6:Y6-4O.

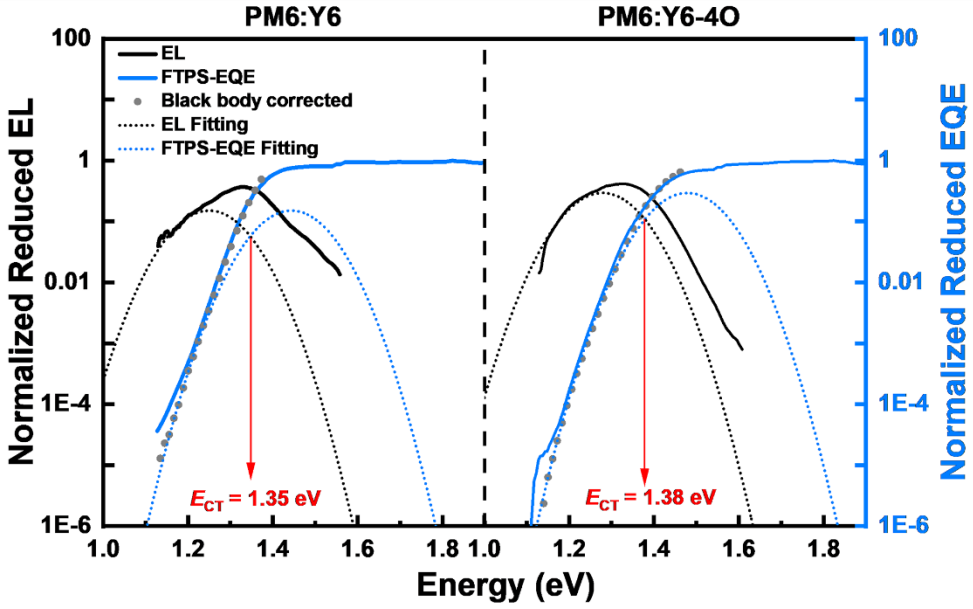

Figure S6. Reduced EL and FTPS-EQE spectra of the as-cast devices based on PM6:Y6 and PM6:Y6-4O processed from toluene.

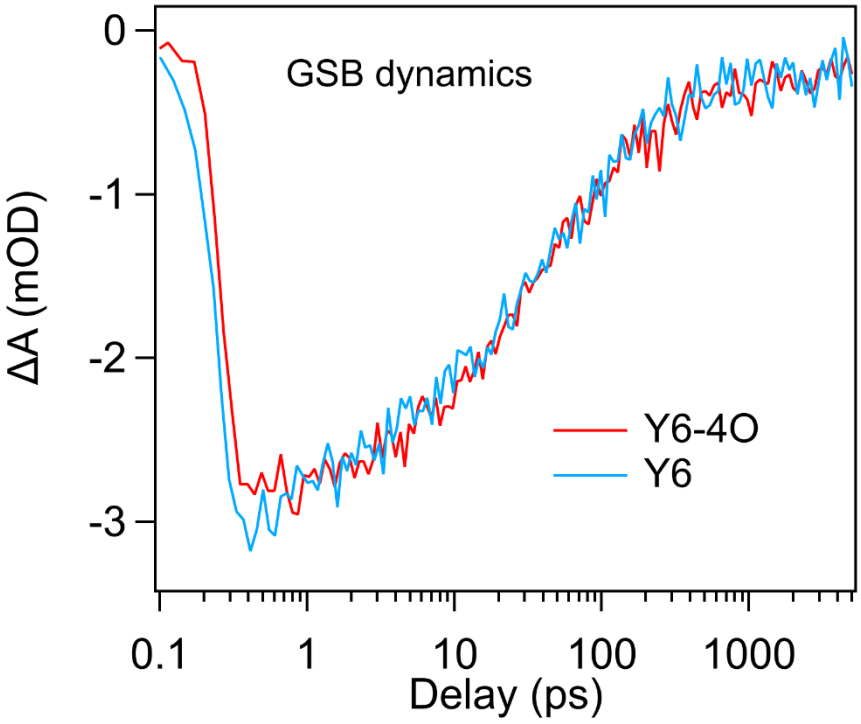

Figure S7. TA kinetics of Y6 and Y6-4O GSB recovery in neat films.

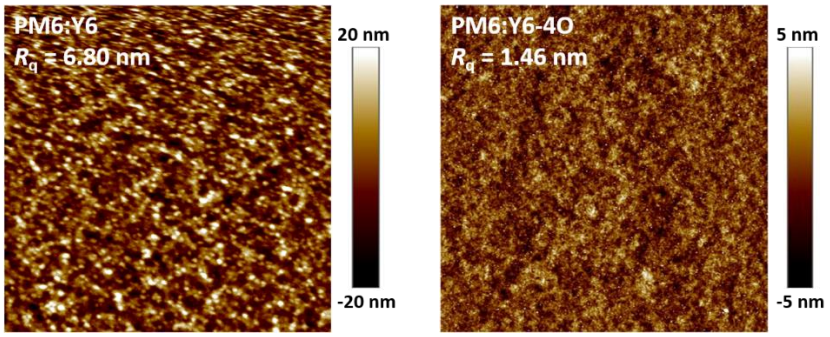

Figure S8. AFM height images of PM6:Y6 and PM6:Y6-4O blend films.

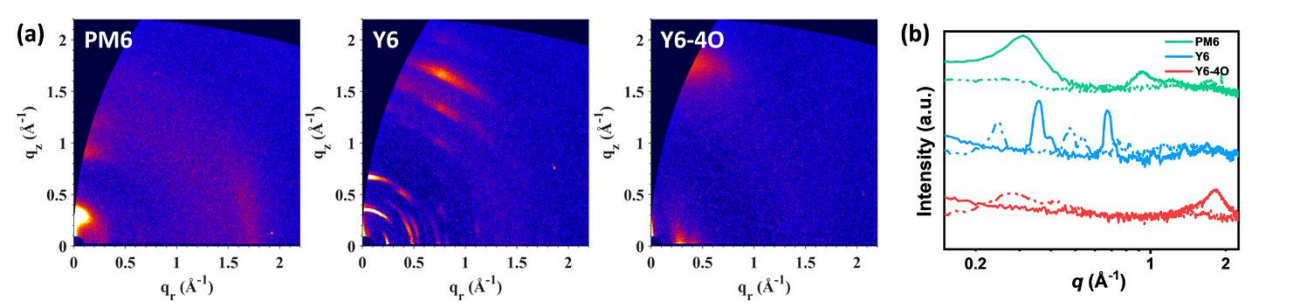

Figure S9. (a) 2D GIWAXS patterns and (b) the scattering profiles of in-plane (dashed line) and out-of-plane (solid line) for PM6, Y6 and Y6-4O neat films.

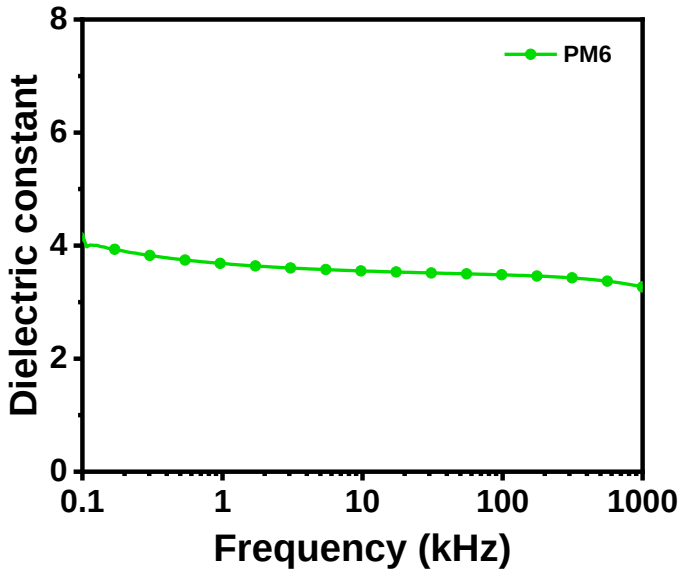

Figure S10. Dielectric constant versus frequency of PM6.

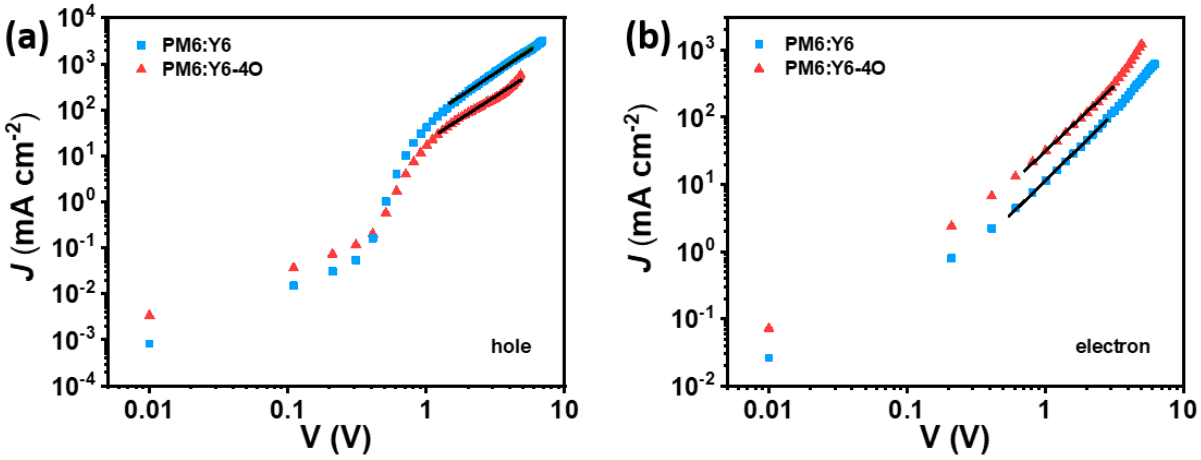

Figure S11. *J-V* characteristics in the dark for (a) hole-only and (b) electron-only as-cast devices processed from toluene based on PM6:Y6 and PM6:Y6-4O.

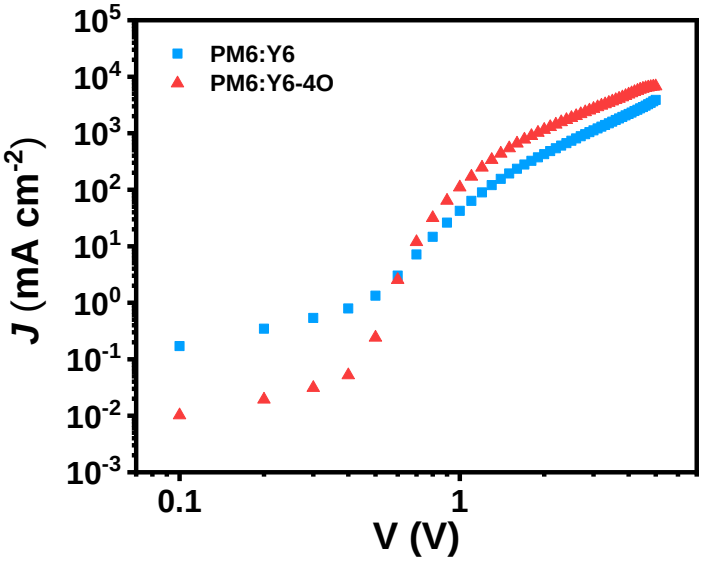

Figure S12. *J-V* characteristics in the dark for double-carrier as-cast devices based on processed from toluene based on PM6:Y6 and PM6:Y6-4O.

Table S1. Photovoltaic Performances of single component OSCs.

Active layer	V_{OC} (V)	J_{SC} (mA cm^{-2})	FF (%)	PCE (%)
Y6	0.794	0.316	30.0	0.075
Y6-4O	0.735	0.476	28.4	0.100

Table S2. Photovoltaic Performances of as-cast OSCs based on PM6:Y6 and PM6:Y6-4O processed from different solvent.

Acceptor	Solvent	V_{OC}[a] (V)	J_{SC}[a] (mA cm^{-2})	FF[a] (%)	PCE[a] (%)
Y6-4O	xylene	0.845 ± 0.001 (0.846)	24.2 ± 0.2 (24.4)	67.9 ± 0.9 (69.0)	13.9 ± 0.2 (14.2)
Y6-4O	THF	0.829 ± 0.001 (0.830)	23.7 ± 0.4 (24.1)	62.4 ± 1.0 (63.3)	12.2 ± 0.3 (12.7)

[a] Average values with standard deviation were obtained from 6 devices and the values in brackets are the parameters of the best device.

Table S3. Summary of the photovoltaic performance based on high dielectric constant organic semiconductors.

Name	Dielectric constant	Active layer	PCE (%)	Ref.
ITIC-OE	9.4	PBDB-T:ITIC-OE	8.5	[4]
ITIC-OEG	5.59 ± 0.78	PPDT2FBT:ITIC-OEG	1.58	[5]
FCN-2	4.9 ± 0.1	PCDTBT:FCN-2	5.55	[6]
FCN-4	4.9 ± 0.1	PCDTBT:FCN-4	3.43	[6]
FCN-6	4.9 ± 0.1	PCDTBT:FCN-6	4.97	[6]
FCN-8	4.9 ± 0.1	PCDTBT:FCN-8	3.50	[6]
M1	8.5	P3HT:M1	0.10	[7]
M2	9.8	P3HT:M2	0.12	[7]
DG	6.1	DG	0.3	[8]
PDPP3T-O14	5.5 ± 0.3	PDPP3T-O14:$PC_{71}BM$	4.52	[9]
PIDT-DPP-CN	5	PIDT-DPP-CN/C_{60}	1.44	[10]
Y6-4O	**5.13**	**PM6:Y6-4O**	**15.2**	**This work**

Table S4. Summary of the photovoltaic performance of the as-cast devices processed using non-halogenated solvent.

Active layer	Solvent	PCE (%)	Year	Ref.
X2:$PC_{61}BC8$	2-MeTHF	4.8	2014	[11]
P1:$PC_{61}BM$	*o*-xylene/MeOH	7.3	2014	[12]
P2:$PC_{61}BM$	*o*-xylene/MeOH	7.5	2014	[12]
P3:$PC_{61}BM$	*o*-xylene/MeOH	7.4	2014	[12]
PBDT-TS1:PPDIODT	anisole	6.58	2016	[13]
PTB7-Th:tPDI-Hex	2Me-THF	4.8	2017	[14]
PffBT4T-2DT:EH-IDTBR	mesitylene	11.1	2017	[15]
BDTSTNTTR:$PC_{71}BM$	CS_2	11.53	2017	[16]
PBDTS-TDZ:ITIC	*o*-xylene	12.80	2018	[17]
PBDT-F-C4T:IT-4F	TMB	11.2	2019	[18]
PM6:Y6-4O	**toluene**	**15.2**	**2021**	**This work**

Table S5. Morphology parameters fitted by GISAXS profiles (ξ is the intermixing domain size; $2R_g$ is the acceptor domain size).

Sample	ξ (nm)	$2R_g$ (nm)
PM6:Y6	51.5	15.8
PM6:Y6-4O	41.4	20.8

References

(1) Yao, J.; Qiu, B.; Zhang, Z. G.; Xue, L.; Wang, R.; Zhang, C.; Chen, S.; Zhou, Q.; Sun, C.; Yang, C.; Xiao, M.; Meng, L.; Li, Y. Cathode engineering with perylene-diimide interlayer enabling over 17% efficiency single-junction organic solar cells. *Nat. Commun.* **2020**, *11*, 2726.

(2) Song, J.; Zhang, M.; Yuan, M.; Qian, Y.; Sun, Y.; Liu, F. Morphology characterization of bulk heterojunction solar cells. *Small Methods* **2018**, *2*, 1700229.

(3) Malliaras, G. G.; Salem, J. R.; Brock, P. J.; Scott, C. Electrical characteristics and efficiency of single-layer organic light-emitting diodes. *Phys. Rev. B: Condens. Matter Mater. Phys.* **1998**, *58*, R13411.

(4) Liu, X.; Xie, B. M.; Duan, C. H.; Wang, Z. J.; Fan, B. B.; Zhang, K.; Lin, B. J.; Colberts, F. J. M.; Ma, W.; Janssen, R. A. J.; Huang, F.; Cao, Y. A high dielectric constant non-fullerene acceptor for efficient bulk-heterojunction organic solar cells. *J. Mater. Chem. A* **2018**, *6*, 395-403.

(5) Jang, B.; Lee, C.; Lee, Y. W.; Kim, D.; Uddin, M. A.; Kim, F. S.; Kim, B. J.; Woo, H. Y. A high dielectric n-type small molecular acceptor containing oligoethyleneglycol side-chains for organic solar cells. *Chin. J. Chem.* **2018**, *36*, 199-205.

(6) Zhang, S.; Zhang, Z. J.; Liu, J.; Wang, L. X. Fullerene adducts bearing cyano moiety for both high dielectric constant and good active layer morphology of organic photovoltaics. *Adv. Funct. Mater.* **2016**, *26*, 6107-6113.

(7) Donaghey, J. E.; Armin, A.; Burn, P. L.; Meredith, P. Dielectric constant enhancement of non-fullerene acceptors via side-chain modification. *Chem. Commun.* **2015**, *51*, 14115-14118.

(8) Armin, A.; Stoltzfus, D. M.; Donaghey, J. E.; Clulow, A. J.; Nagiri, R. C. R.; Burn, P. L.; Gentle, I. R.; Meredith, P. Engineering dielectric constants in organic semiconductors. *J. Mater. Chem. C*

2017, *5*, 3736-3747.

(9) Chen, X.; Zhang, Z.; Ding, Z.; Liu, J.; Wang, L. Diketopyrrolopyrrole-based conjugated polymers bearing branched oligo(ethylene glycol) side chains for photovoltaic devices. *Angew. Chem., Int. Ed.* **2016**, *55*, 10376-10380.

(10)Cho, N.; Schlenker, C. W.; Knesting, K. M.; Koelsch, P.; Yip, H. L.; Ginger, D. S.; Jen, A. K. Y. High-dielectric constant side-chain polymers show reduced non-geminate recombination in heterojunction solar cells. *Adv. Energy Mater.* **2014**, *4*, 1301857.

(11)Chen, X.; Liu, X.; Burgers, M. A.; Huang, Y.; Bazan, G. C. Green-solvent-processed molecular solar cells. *Angew. Chem., Int. Ed.* **2014**, *53*, 14378-14381.

(12)Deng, Y. F.; Li, W. L.; Liu, L. H.; Tian, H. K.; Xie, Z. Y.; Geng, Y. H.; Wang, F. S. Low bandgap conjugated polymers based on mono-fluorinated isoindigo for efficient bulk heterojunction polymer solar cells processed with non-chlorinated solvents. *Energy Environ. Sci.* **2015**, *8*, 585-591.

(13)Li, S. S.; Zhang, H.; Zhao, W. C.; Ye, L.; Yao, H. F.; Yang, B.; Zhang, S. Q.; Hou, J. H. Green-solvent-processed all-polymer solar cells containing a perylene diimide-based acceptor with an efficiency over 6.5%. *Adv. Energy Mater.* **2016**, *6*, 1501991.

(14)Dayneko, S. V.; Hendsbee, A. D.; Welch, G. C. Fullerene-free polymer solar cells processed from non-halogenated solvents in air with pce of 4.8. *Chem. Commun.* **2017**, *53*, 1164-1167.

(15)Wadsworth, A.; Ashraf, R. S.; Abdelsamie, M.; Pont, S.; Little, M.; Moser, M.; Hamid, Z.; Neophytou, M.; Zhang, W. M.; Amassian, A.; Durrant, J. R.; Baran, D.; McCulloch, I. Highly efficient and reproducible nonfullerene solar cells from hydrocarbon solvents. *ACS Energy Lett.* **2017**, *2*, 1494-1500.

(16)Wan, J. H.; Xu, X. P.; Zhang, G. J.; Li, Y.; Feng, K.; Peng, Q. Highly efficient halogen-free

solvent processed small-molecule organic solar cells enabled by material design and device engineering. *Energy Environ. Sci.* **2017**, *10*, 1739-1745.

(17) Xu, X.; Yu, T.; Bi, Z.; Ma, W.; Li, Y.; Peng, Q. Realizing over 13% efficiency in green-solvent-processed nonfullerene organic solar cells enabled by 1,3,4-thiadiazole-based wide-bandgap copolymers. *Adv. Mater.* **2018**, *30*, 1703973.

(18) Guo, H.; Zhang, Y. D.; Chen, L.; Liao, X. F.; Xie, Q.; Cui, Y. J.; Huang, B.; Yang, C.; Chen, Y. W. Non-halogenated-solvent-processed highly efficient organic solar cells with a record open circuit voltage enabled by noncovalently locked novel polymer donors. *J. Mater. Chem. A* **2019**, *7*, 27394-27402.